

## Simulation and Analysis on Machining Channels in the Electrochemical Pattern Transfer Method

Zhe Wang, Shuangqing Qian\*, Hongbei Cao, Hua Zhang, Kai Bao

School of Mechanical Engineering, Nantong university, Nantong 226019, P. R. China

\*E-mail: [sqqian@ntu.edu.cn](mailto:sqqian@ntu.edu.cn)

*Received:* 30 March 2016 / *Accepted:* 11 April 2016 / *Published:* 4 June 2016

---

Proton exchange membrane fuel cell (PEMFC) is considered as a preferred clean and efficient energy, and its flow channel structure design and forming technology directly affect the efficiency of power generation. In this work, the shape evolution of flow channels in electrochemical pattern transfer machining (ECPTM) was studied carefully and the influences of machining time, inter-electrode gap, insulation thickness, and opening and spacing ratio of channel on the electric field distribution and processing localization were investigated numerically. The results demonstrated that the insulation thickness had almost no effect on the electric field distribution, whereas the inter-electrode gap showed an important influence on both electric field distribution and processing localization. When the opening and spacing ratio of channel was more than 1:3, there were no interferences between channels and a higher spatial resolution could be obtained in both simulation and experiment.

---

**Keywords:** Flow channel; Electrochemical pattern transfer; Finite element simulation; Localization; Spatial resolution;

### 1. INTRODUCTION

As a preferred clean and efficient energy, proton exchange membrane fuel cell (PEMFC) has currently become the ideal power source for electric cars as well as military and civil applications, which shows extensive prospects in the 21st century [1]. Metallic bipolar plates, the key components of PEMFC, can connect individual cells together in series and provide the gas reaction field by flow channels[2]. The forming process of metallic bipolar plates with flow field involves plastic forming technology [3-5], liquid forming technology [6] and non-traditional machining technology [7, 8]. With the miniaturization of fuel cells for 3C applications, it is more and more difficult to form thinner bipolar plates through existing methods.

Electrochemical machining (EMM) is a controlled anodic dissolution process. It is suitable for forming thinner metallic plates due to its significant advantages such as no tool wear, free stress, high throughput and high ability to machine complex shapes regardless of their stiffness, strength and toughness [9]. A number of scholars tried to create micro-holes or microgrooves by through-mask electrochemical micro-machining (TMEMM) [10, 11]. But this method increased the processing cost considering the manufacturing and removing operations of the photoresist patterned metal workpiece. I. Schonenberge [12] proposed ECPTM firstly to solve the problems of TMEMM and successfully produced microgrooves of 120  $\mu\text{m}$  in width and 1.5  $\mu\text{m}$  in depth on the surface of copper. Afterwards, Qu [13] gained micro-dimples array of 109.4  $\mu\text{m}$  in diameter and 15.1  $\mu\text{m}$  in depth on the surface of piston. Wang [14] created turbulated cooling holes of 0.45 mm in height of rib on the gas turbine blade. H.L. Costa [15] produced micro-dimples array of 120  $\mu\text{m}$  in diameter and 50  $\mu\text{m}$  in depth on the steel. W. Lang [16] successfully obtained microgrooves of 7.5 mm in width and less than 10  $\mu\text{m}$  in depth on the steel.

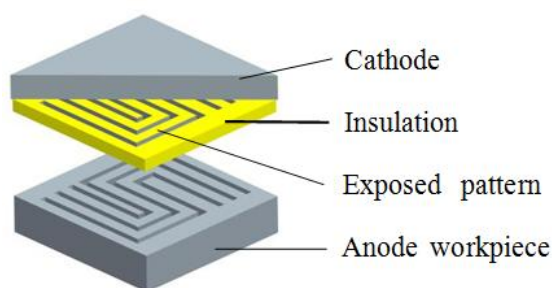


**Figure 1.** Schematic of electrode arrangement

Figure 1 shows schematic of electrode arrangement in ECPTM. Since it is difficult to detect the electric field distribution between anode and cathode and to track the shape evolution in experiment, finite element simulation and analysis on machining channels of metallic bipolar plates in ECPTM with a mask onto the cathode are carried out in this work.

**2. MAIN PRINCIPLES AND SHAPE EVOLUTION MODELING**

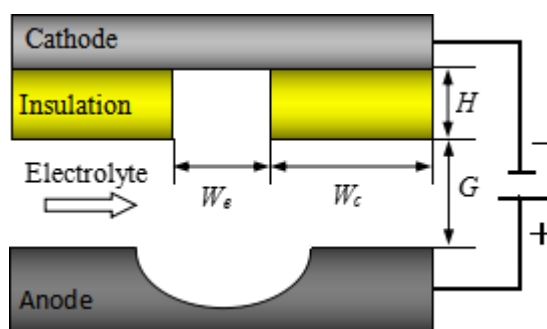


**Figure 2.** Schematic of ECPTM

Figure 2 illustrates the schematic of simplified ECPTM process, the photoresist patterned metal is chosen as the cathode and other metal workpieces are as the anode in an electrochemical cell. The

metal workpiece opposite to the exposed metal surface of the cathode is removed by high-rate anodic metal dissolution through applying an external current. H<sub>2</sub> that evolves at the exposed metal surface of the cathode and the products generated at the anode are taken away by the high-speed flow of electrolyte between electrodes. Therefore, the exposed patterns on the cathode are transferred into the anode locality. Its localization is mainly decided by the current density distribution [17], which is may influenced by the insulation thickness *H*, the inter-electrode gap *G*, the width of exposed insulation *W<sub>e</sub>* and the width of covered electrode surface *W<sub>c</sub>*.

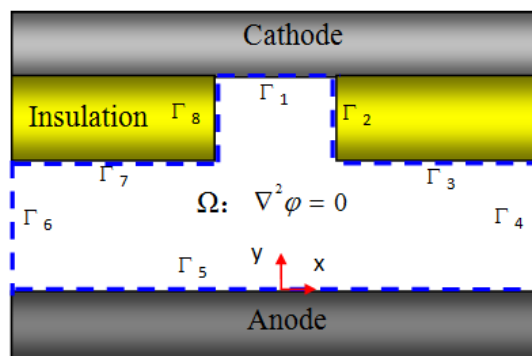


**Figure 3.** Electric potential distribution in the inter-electrode gap

The calculative model should be built to obviously observe the current density distribution. For the convenience of numerical calculation, some assumptions are made as follows: 1) The current density distribution at the anode surface is determined solely by the Ohmic effects and the electrodes are defined as equipotential surfaces; 2) the process of ECM is in the equilibrium state; 3) the electrical parameters do not change with time; 4) the conductivity and temperature of electrolyte are uniform and the concentration gradient of the electrolyte is negligible. The electric potential distribution in the inter-electrode gap has been obtained, as shown in Figure 3.

The potential  $\phi$  obeys Laplace’s equation within gap domain  $\Omega$ :

$$\nabla^2 \phi = \frac{\partial^2 \phi}{\partial x^2} + \frac{\partial^2 \phi}{\partial y^2} = 0 \tag{1}$$

Boundary conditions are as follows:

$$\phi|_{\Gamma_1} = U \text{ (at the anode surface)} \tag{2}$$

$$\phi|_{\Gamma_5} = 0 \text{ (at the cathode surface)} \tag{3}$$

$$\frac{\partial \phi}{\partial \mathbf{n}} \Big|_{\Gamma_{2,3,4,6,7,8}} = 0 \text{ (the additional condition)} \tag{4}$$

In ECM, the current distribution determines the profile of channels. The shape of workpiece is determined by the material removal rate on machining surface. The material removal rate depends on the current density based on potential drop on the material geometry profile, which also changes with the machining times due to the renew of anode profile. According to Faraday's law, the metal removal rate  $v_a$  can be described by:

$$v_a = \eta \omega i = \eta \omega \kappa E \tag{5}$$

where  $\eta$  is the current efficiency,  $\omega$  is the volume electrochemical equivalent of the material,  $k$  is the conductivity of electrolyte,  $E$  is the electric field intensity, and  $i$  is the current density. In the process of ECPTM, the coordination of one initial point  $P_0$  on the surface of anodel changes according to the theory of electric field principle. Assuming  $P_i$  is the point after the machining time  $T$ , then  $P_{i+1}$  is the next point of  $P_i$  after the step time  $\Delta t$ . The recursion formula is as follows:

$$\begin{cases} x_{i+1} = x_i + \vec{v}_{ax} \cdot \Delta t = x_i + \eta\omega\kappa\vec{E}_x \cdot \Delta t \\ y_{i+1} = y_i + \vec{v}_{ay} \cdot \Delta t = y_i + \eta\omega\kappa\vec{E}_y \cdot \Delta t \end{cases} \quad (i=0,1,2,3\dots) \quad (6)$$

where  $\vec{E}_x$  and  $\vec{E}_y$  are vector values of electric field and  $\Delta t$  is the step time.

The relationship  $\eta-i$  can be obtained by experiment in 18%  $\text{NaNO}_3$  solution at  $30^\circ\text{C}$  as follows[17]:

$$\eta = -14.06313 + 1.34332i + 0.01978i^2 - 4.53599 \times 10^{-4}i^3 + 2.14043 \times 10^{-6}i^4 \quad (7)$$

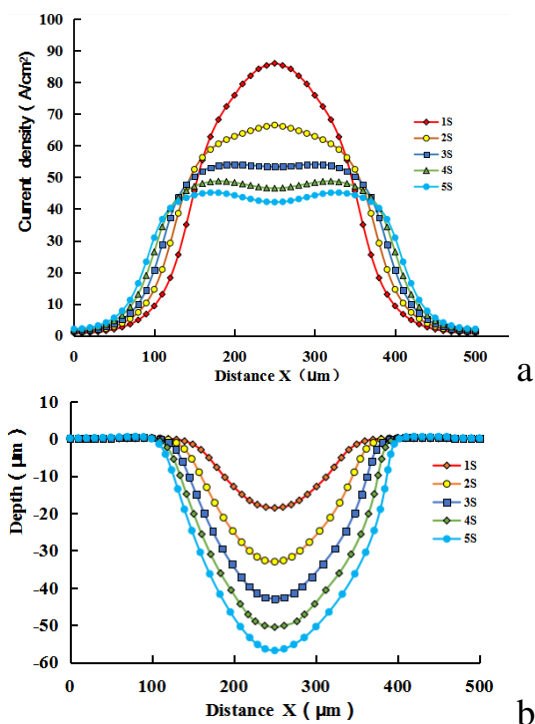
The processing localization is measured by the corrosion coefficient EF as:

$$EF = \frac{d}{W_{se} - W_e / 2} \quad (8)$$

It can be concluded that the processing localization can be improved with the increase of EF. In this work, the influences of different parameters on localization will be measured by EF.

### 3. SIMULATION RESULTS AND DISCUSSION

#### 3.1 Effect of machining time on channel evolution



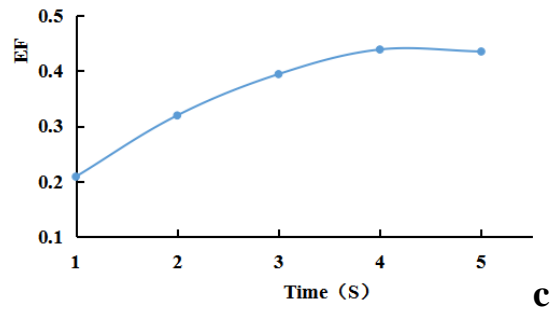


**Figure 4.** Effect of machining time on the machined single channel: **a** current density on initial anode surface; **b** depth of channel; **c** EF of channel

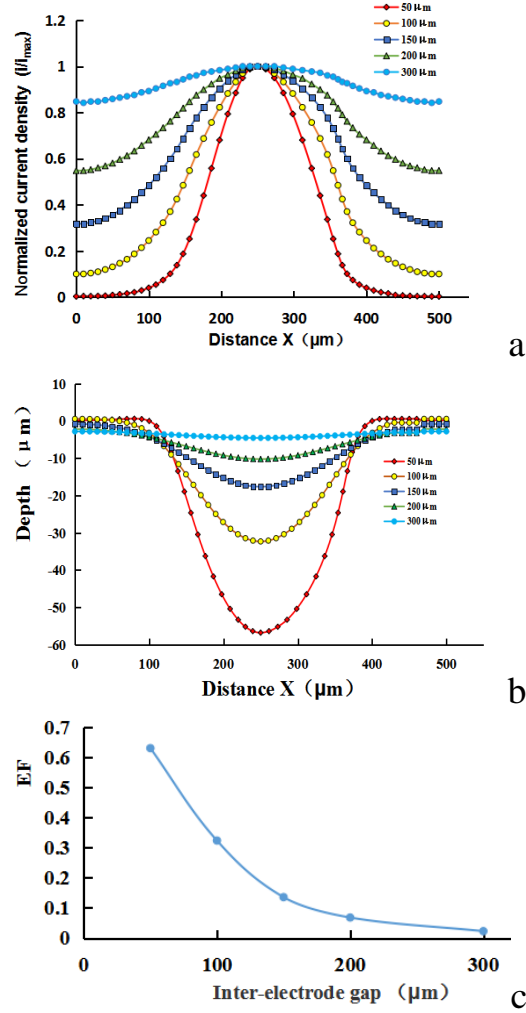


**Figure 5.** Effect of inter-electrode gap on the machined single channel: **a** normalized current density on initial anode surface; **b** depth of channel; **c** EF of channel

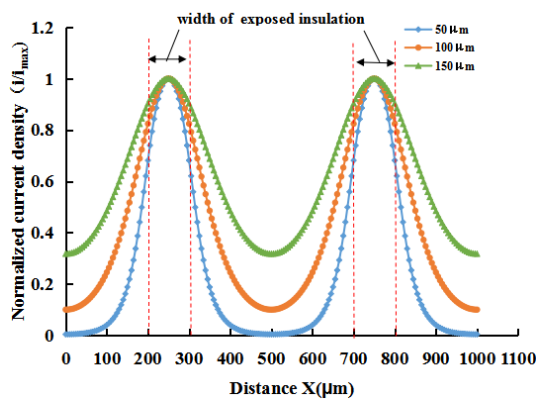


**Figure 6.** Normalized current density on initial anode surface at various inter-electrode gaps (two channels)

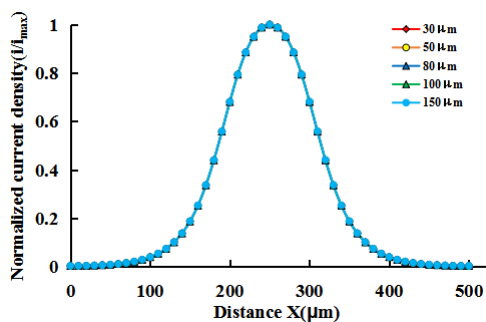


**Figure 7.** Normalized current density at initial anode surface at various insulation thicknesses

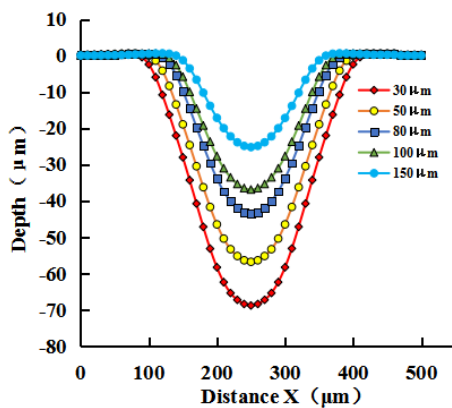


**Figure 8.** Effect of variance of insulation thickness on depth of channel

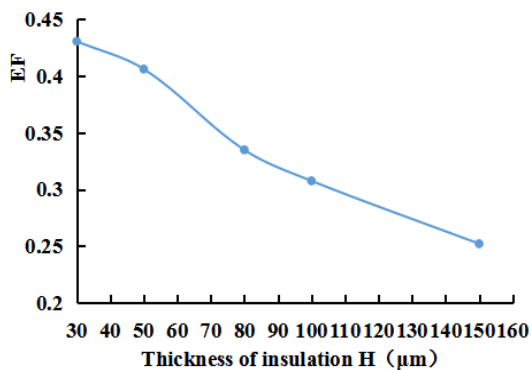


**Figure 9.** Effect of variance of insulation thickness on EF

In order to investigate the current density distribution and predict the shape evolution of flow channel with machining time. The boundaries are progressively updated every time step of 0.2S by using ANSYS Parametric Design Language (APDL) under the following conditions:  $W_e=100\mu\text{m}$ ,  $W_c=200\mu\text{m}$ ,  $H=50\mu\text{m}$ ,  $U=9\text{V}$ ,  $G=50\mu\text{m}$  and machining time is 5S.

Figure 4 a) shows the numerical simulation results of the current density distribution on the workpiece surface, and Figure 4 b) presents the program flow diagram that simulates the shape evolution. With the material dissolution, a given cavity evolves from a flat shape into a arc shape. At the beginning, the removal of materials only occurs along the Y direction of the workpiece. The removal rate is non-uniform because of the non-uniform current density distribution on the workpiece, which results in a convex bottom of the channel. With the increase of machining time, material removal in the side of the micro-channel along the X direction of the workpiece occurs in spite of removal rate is relatively slow. Meanwhile, material removal along the Y direction of the workpiece also occurs. As a result, the profile of the channel evolves from a flat shape into a arc shape, which leads to the uniform current density distribution in Figure 4 b) lastly. This result is agreed with the report by Qu [13] and S.Nourai [18]. Qu indicated that the arc shape of dimples simulated in the numerical calculation were matched with those obtained in the experiments due to non-uniform current density on the workpiece. S.Nourai reported the sinusoidal profile of the anode after 90S of active electrodisolution in the simulation. As shown in Figure 4 c), The value of EF increases rapidly when the time less than 4S, which indicates the rapid improvement of localization. However, EF decreases slowly with the time when the time more than 4S. Therefore, precise machining time should be chosen to machine channel so as to achieve better localization.

### 3.2 Effect of inter-electrode gap on channel machining

By the finite element method (FEM), the current density on the workpiece surface in electrolyte has been simulated by ANSYS with the scales of  $G=50\mu\text{m}$ ,  $100\mu\text{m}$ ,  $150\mu\text{m}$ ,  $200\mu\text{m}$  and  $300\mu\text{m}$  under the conditions as before. Figure 5 a) shows the normalized current density distribution on the initial anode surface. The normalized current density is defined as  $i/i_{\text{max}}$ , where  $i_{\text{max}}$  represents the maximum current density and  $i$  represents the current density of every key point on the surface. The current density distribution on each surface is uneven, and it decreases rapidly from the center of the channel where the highest current density always appears. The smaller the  $G$  is, the more non-uniform the current density distribution, which leading to a convex dimple profile. As Figure 5 b) shows, the depth of channel become higher and higher with the decrease of  $G$ , and the channel side is etched lower due to the bigger current density difference on the anode surface. With the sharp decrease of  $G$ , EF increases rapidly in Figure 5 c), which indicates the rapid improvement of localization. To sum up, the optimum inter-electrode gap  $G$  is determined to be  $50\mu\text{m}$ . The experiments results made by S.Roy [12] showed an optimised distance between the anode and cathode are essential for good pattern transfer and the microscale patterns, namely  $50\mu\text{m}$ ,  $100\mu\text{m}$ ,  $200\mu\text{m}$ , could be transferred into the substrate with good reproducibility when the inter-electrode gap being  $500\mu\text{m}$ . But the depth of channels were  $1.5\mu\text{m}$  merely.

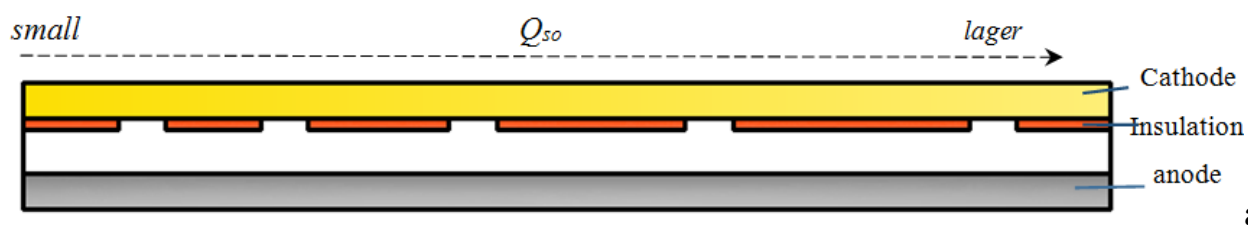
The spatial resolution of channel may be affected by the inter-electrode gap when the transferred patterns are array of flow channels arranged in a distance of  $400\mu\text{m}$  instead of a single channel. As shown in Figure 6, the electric field distribution on anode surface, which is adverse to the exposed insulation, keeps independent of each other when  $G$  is  $50\mu\text{m}$ ; however, distinguished interferences between channels appear when  $G$  is more than  $50\mu\text{m}$ , which create unwanted channels with low spatial resolution and over-etch the interval space of channels. Therefore, smaller inter-electrode gap should be chosen to machine array of patterns so as to achieve higher spatial resolution and better localization. This result is in agreement with the reports by C.Winkemann [16], which reported smaller inter-electrode gaps increase the spacial resolution of the transfered structure and  $75\mu\text{m}$  wide gaps integrated into the cathode were not transfered to the substrates because of higher stray electric field due to the inter-electrode gap being  $100\mu\text{m}$  away.

### 3.3 Effect of insulation thickness on channel machining

In order to optimize the insulation thickness, the influence of insulation thickness on the etched channel profile has been simulated. Here, the inter-electrode gap  $G$  is set to  $100\mu\text{m}$ , the insulation thickness  $H$  is respectively set to  $30\mu\text{m}$ ,  $50\mu\text{m}$ ,  $80\mu\text{m}$ ,  $100\mu\text{m}$  and  $150\mu\text{m}$ , and others simulation parameters are the same as before.

Figure 7 shows the normalized current density distribution on the initial anode workpiece surface with different insulation thicknesses. No matter what the insulation layer thickness is, the current density distribution keeps unchanged but only the current density value varies. The current density peaks appear at the center of the channel and decrease rapidly from the center. As shown in Figure 8, the depth and width of the channel both increase with the decrease of insulation thickness. However, the shape of channels are not changed with various insulation thickness. This results is in agreement with the reports by Qu [13] and Qian [17], which both indicated that the thickness of dry film or SU8 photosensitive resist had no effect on the etching profile of dimples. Figure 9 shows the variation of EF with the thickness of insulation layer. It can be seen that smaller  $H$  can result in higher localization of channel due to the influence of  $H$  instead of  $G$  on the distance of electrodes ( $H+G$ ) in practice. On the other hand, when the insulation thickness is too small, it is difficult to expel  $H_2$  and other products by the high-speed flow of electrolyte between electrodes so that traffic jam may happen in inter-electrode sometimes, which will prevent electrolytic reaction and burn up the texture surface of channel. In view of this, it prefers to choose the smallest insulation thickness on the premise of no traffic jam in electrolyte.

### 3.4 Effect of $W_e/W_c$ on channel machining



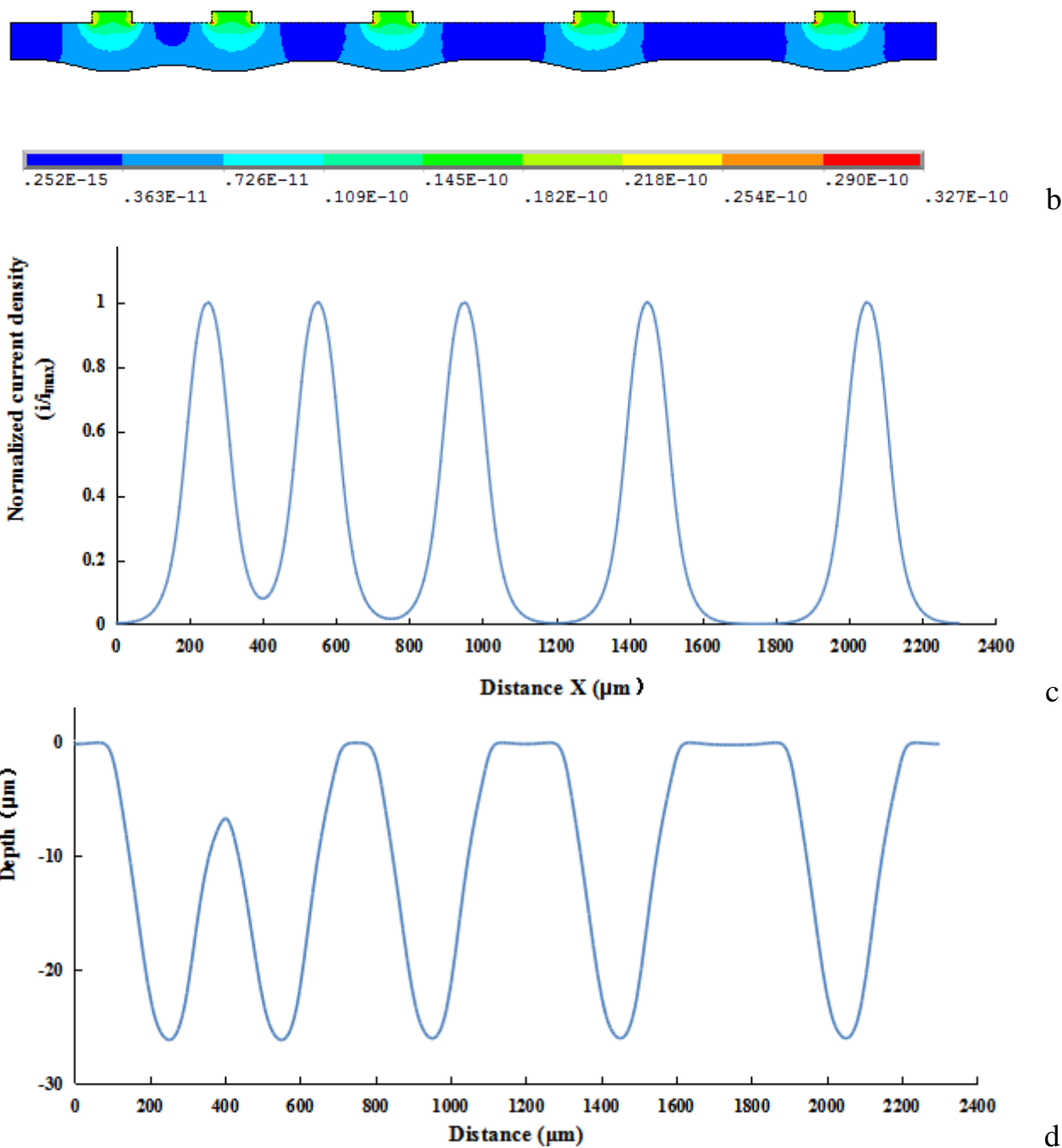


**Figure 10.** Effect of variance of  $Q_{so}$  on current distribution and depth of channel: **a** computation model; **b** Electric field intensity cloud image; **c** normalized current density; **d** the cross-section shape of channels

The opening and spacing ratio of exposed pattern on the cathode can be defined as  $Q_{so} = W_e/W_c$ . In order to optimize  $Q_{so}$ , the influence of insulation layer on the etched channel profile has been simulated (Figure 10 a)). Here, the  $W_e$  is set to 100  $\mu m$ .  $W_c$  is respectively set to 200 $\mu m$ , 300 $\mu m$ , 400 $\mu m$  and 500 $\mu m$ .  $G$  is set to 100 $\mu m$  and  $H$  is set to 30 $\mu m$  in the model, and other simulation parameters are the same as before.

Figure 10 b) and d) show part of simulation results on the electric field intensity distribution and the cross-section shape of the channels, respectively. Figure 10 c) shows the normalized current density distribution on the initial anode workpiece surface. As can be seen, the current density distribution on the initial metal surface is highly non-uniform and the maximum current density occurs at the center of metal surface opposite to the exposed insulation of cathode. Besides, there are obvious interferences of feature between channels due to the interference of current density. The spatial resolution is lower when  $Q_{so}$  is less than 1:3, which results in a highly uneven etched profile and unwanted performance. When  $Q_{so}$  is more than 1:3, the above interference does not occur and the spacing between channels is not over-etched. On the whole, the spatial resolution of channels can be improved rapidly with the increase of  $Q_{so}$ . The formed channels with the width of  $243.93\mu\text{m}$  and depth of  $25.85\mu\text{m}$  was presented in Figure 10 d). The similar report made by S.Nouraei [18] showed there were no pattern being transferred into the substrate in the condition of inter-electrode gap was about  $300\mu\text{m}$  when  $W_e$  and  $W_c$  were set at  $50$  and  $350\mu\text{m}$  respectively. However, etched depth  $4.7\mu\text{m}$  were obtained when the  $W_e$  and  $W_c$  were set at  $50$  and  $700\mu\text{m}$  respectively. Which is in agreement with this report that the opening and spacing ratio of channel on the cathode have an effect on the spatial resolution and depth of transferred channel in the cathode.

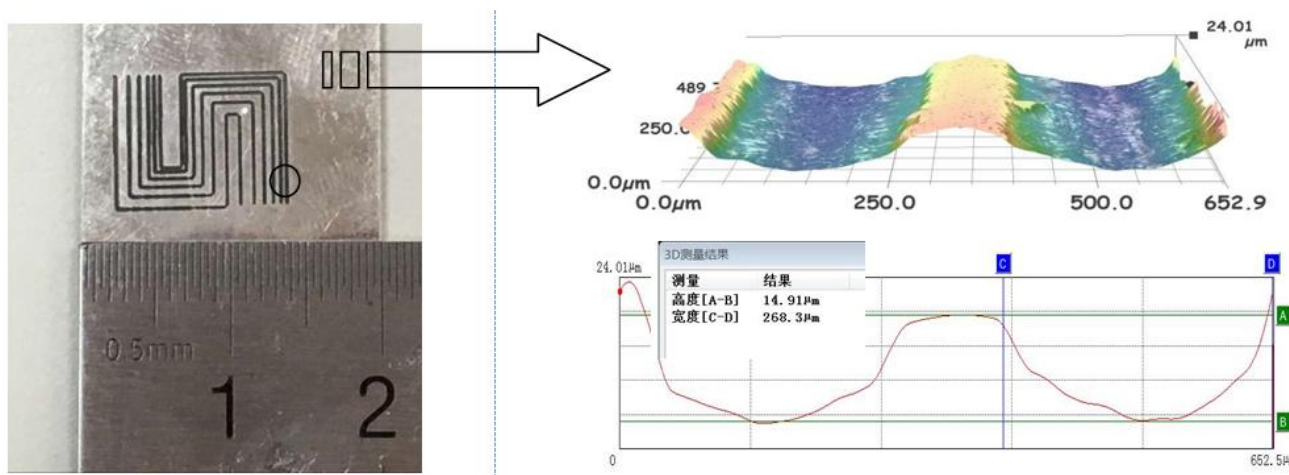


**Figure 11.** Profiles of channels: **a** machined channel; **b** 3D optical profile and cross-sectional shape

For comparing the simulation results, the machining channels of metallic bipolar plates for PEMFC in ECPTM are investigated experimentally. Figure 11 shows the eroded anode profile and the cross-section profile of the channels that is observed through ultra-depth 3D microscope (VHX-2000, Keyence, Japan) after 5S machining time with a voltage of 9V and an inter-electrode gap size of  $100\mu\text{m}$  in 18%  $\text{NaNO}_3$  solution at room temperature. As can be seen, when  $Q_{so}$  is 1:3, there are no interferences between channels with the width of  $268.3\mu\text{m}$  and depth of  $14.91\mu\text{m}$ . Accordingly good agreement between theory and experimental data verified the validation and results of the computer simulation of the channel evolving in ECPTM. However, the simulation results of width and depth of channel deviate from experimental data slightly. This phenomenon can be attributed to the fact that actual current density distribution is influenced by various complex factors such as the transient

change of inter-electrode gap with the time, the instantaneous change of the electrolyte temperature and conductivity, the electrolyte flow field distribution and the transfer of electrolytic products by electrolyte. Nevertheless, the simulation results can still roughly reflect the forming trend of the channels in ECPTM.

#### 4. CONCLUSIONS

In summary, finite element simulation and analysis on the machining channel of metallic bipolar plates in ECPTM with a mask onto the cathode were carried out in this work, and the influences of machining characteristics on the electric field distribution and processing localization were investigated. Some conclusions can be drawn as follows:

1. The inter-electrode gap has an important influence on the electric field distribution and localization. Smaller inter-electrode gap in machining array of patterned channels can result in higher spatial resolution and localization.

2. With the increase of machining time, the current density distribution becomes more and more uniform on the surface of etched channels and the depth and width of channels become higher and higher.

3. The current density distribution on the initial anode workpiece surface keeps unchanged with the variation of insulation thickness. It prefers to choose smaller insulation thickness on the premise of no traffic jam in electrolyte so as to achieve higher localization.

4. According to simulation and experiment results, the spacing between channels can be properly etched when  $Q_{so}$  is more than 1:3, and the spatial resolution of channels can be improved rapidly with the increase of  $Q_{so}$ .

#### ACKNOWLEDGEMENTS

This work was supported by the National Natural Science Funds (51305212), A Project Funded by the Priority Academic Program Development of Jiangsu Higher Education Institutions and Master's Science and Technology Innovation program of Nantong University(YKC15008).

#### References

1. H.J. Ni, X.X. Wang, M.Y. Huang, F. Li, *Materials Science and Technology*, 2(2008)250.
2. L.J. Yang, H.J. Wei, L. Zhu, X.Y. Jian, Z. Wang, *Metallic Function Materials*, 5(2009)50.
3. Y. Liu, H. Lin, *J. Power Sources*, 195 (2010)3529.
4. J.C. Hung, C.C. Lin, *Journal of Power Sources*, 206(2012)179.
5. J. Shang, L. Wilkerson, S. Hatkevich, G.S. Daehn, *Institut für Umformtechnik-Technische Universität Dortmund*, (2010).
6. C.K. Jin, C.G. Kang, *Journal of Power Sources*, 196(2011), 8241.
7. J.C. Hung, D.H. Chang, C.Yin, *Journal of Power Sources*, 198 (2012)158.
8. S.J. Lee, C.Y. Lee, K.T. Yang, *Journal of Power Sources*, 185(2008) 1115.
9. A.E. Fetohi, R.M.A. Hameed, K.M. El-Khatib, E.R. Souaya, *Int. J. Hydrogen Energy*, 37(2012)10807.
10. X.L. Chen, N.S. Qu, H.S. Li, *Int. J. Advanced Manufacturing Technology*, 80(2015)1.

11. S.Q. Qian, F. Ji, N.S. Q, H.S. Li, *Materials & Manufacturing Processes*, 29 (2014)1488.
12. I. Schönenberger, S. Roy, *Electrochimica Acta*, 51(2005)809.
13. N.S. Qu, X.F. Zhang, X.L. Chen, H.S. Li, D.Zhu, *J. Materials Processing Technology*, 218(2015)71.
14. M. Chen, M.H. Wang, W. Peng, *Mechanical & Electrical Engineering Magazine*, 26(2009)87.
15. H.L. Costa, I.M. Hutchings. *Journal of Materials Processing Technology*, 209(2009)3869.
16. C. Winkelmann, W. Lang, *International Journal of Machine Tools & Manufacture*, 72(2013)25.
17. S.Q. Qian, D. Zhu, H.S. Li, S. M, *Transactions of CSICE*, 28(2010)173.
18. S. Nouraei, S. Roy, *Journal of The Electrochemical Society*, 2(2008)155.

© 2016 The Authors. Published by ESG ([www.electrochemsci.org](http://www.electrochemsci.org)). This article is an open access article distributed under the terms and conditions of the Creative Commons Attribution license (<http://creativecommons.org/licenses/by/4.0/>).